First principles theoretical modeling of the isomer shift of Mossbauer spectra

Kurian, Reshmi

Chapter 7

Theoretical investigation of hyperfine parameters of iron-based superconductors

Synopsis

The aim of the present chapter is to study the the influence of the structural variation on the isomer shift and magnetic hyperfine coupling constants in iron based superconductors. The calculations based on the linear response approach indicate a decrease of the electron contact density near the ^{57}Fe nucleus with the tetragonal-orthorhombic phase transition in iron pnictides and chalcogenides. Thus, such a decrease of the contact density and corresponding increase of ^{57}Fe isomer shifts can be used for the identification of the local chemical environment in these compounds. The isotropic hyperfine coupling constant A_{iso} of the studied iron based superconductors did not make noticeable differences with the structural phase transition. However, with the inclusion of spin-orbit corrections in the calculations the A_{iso} values make distinct variation between different types of these compounds. The SO corrections scale up to 30 % of the calculated A_{iso} values, and is necessary for the accurate description of magnetic properties in these compounds.

7.1 Introduction

The discovery of high-temperature superconductivity (HTSC) in iron-based compounds has initiated a considerable research activity comparable or even in excess to the discovery of HTSC in cuprates [22]. Iron-based superconductors belong to pnictide (compounds of group V elements) [23–25] or chalcogenide (compounds of group VI elements) class of compounds [26]. One can distinguish several types of iron- based superconductors: a) the REFeAsO systems with RE = Rare Earth = La, Nd, Ce, etc (see Figure 7.1(d)). These compounds are often denoted as "1111" type and become superconducting upon doping with fluorine. For these compounds, the maximum critical temperature Tc = 56 K was achieved for samarium oxyarsenide. b) The "122" systems with the formula AFe_2As_2 (A = Ba, Sr, Ca) (see Figure 7.1(c)) which have critical temperature comparable to the 1111 compounds, the superconductivity emerges with the appropriate substitution of bivalent A cations with monovalent alkali metals, K, Cs *etc.* c) The 111 compounds with the formula LiFeAs and Tc =18K (see Figure 7.1(b)). d) The 011 chalcogenides FeSe with Tc $\approx$ 8.5 K (see Figure 7.1(a)). Most of these systems become superconducting upon doping or application of external pressure.

These compounds contain structures with layers of edge-sharing FeX (X = As, Se, etc.) tetrahedra separated by metal ions. The undoped 1111 compounds, which are non-superconducting, exhibit structural, tetragonal-orthorhombic phase transition upon cooling below 90K and a long-range magnetic order that sets in at the temperature of the structural transition [133]. Other compounds, notably 011 type, do not show any long-range magnetic order although undergo the structural transition [26]. It is worth to mention that for LiFeAs, no

evidence of a structural phase transition is observed so far [134]. Although the relationship between the structure, magnetism and superconductivity is still unresolved, there are claims that the suppression of both the structural transition and magnetic order, or only the magnetic order, or neither are necessary for superconductivity to emerge [135].

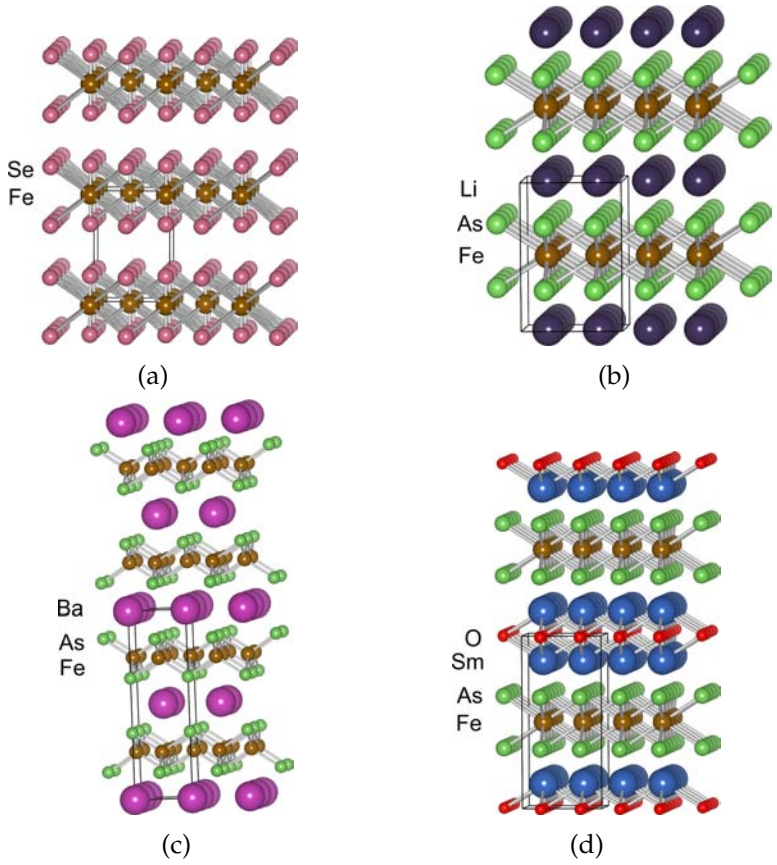

Figure 7.1: *The iron-based superconductors, (a)FeSe (011 type) (b) LiFeAs (111 type)(c) $BaFe_2As_2$ (122 type) (d) LaFeAsO (1111 type).*

All iron based superconductors have a two dimensional (2-D) structure, which is shown in Figure 7.1. Therefore, at a glance their physical

properties are considered to be highly two-dimensional. In resolving the origin of superconductivity in these iron based compounds, the knowledge of their local geometry and local electronic structure is extremely important. The parameters of Mössbauer spectra, such as the isomer shift, quadrupole splitting and magnetic hyperfine splitting, carry information on the spin- and oxidation state of the resonating atom and its local chemical environment. This technique can be used on amorphous/disordered systems and one can monitor phase transitions, mixed phases, disordered structures *etc.* The aim of the present chapter is to find a relation between the local chemical environment of the iron based superconductors and the Mössbauer parameters, isomer shifts and hyperfine coupling constants. This analysis will give us an idea on how can these Mössbauer parameters be used to judge the structure of the iron based superconductors, especially under phase transitions and upon doping/chemical substitutions.

7.2 Details of calculations

The iron chalcogenides and iron pnictides studied are, FeSe, LiFeAs (111 type), $BaFe_2As_2$ (122 type) and SmOFeAs (1111 type). The following geometries were used in this study.

The iron chalcogenide, FeSe crystallizes in tetragonal (P4/nmm) structure at 298 K and in orthorhombic structure (Cmma) at 4 K, composing a stack of edge-sharing $FeSe_4$ tetrahedra with no intercalation layer [26]. The considered cluster is $[FeSe_4]^{6-}$ (see Figure 7.2(a)). LiFeAs crystallizes in tetragonal unit cell (P4/nmm) and there is no structural phase transition with the lowering of temperature. The cluster considered is $[Li_4FeAs_4]^{6-}$ (see Figure 7.2(b)).

The 122 iron pnictide, $BaFe_2As_2$ crystallizes in tetragonal (14/mmm) structure at 298 K where the crystal contains layers of edge-sharing FeAs4/4 tetrahedra separated only by barium atoms [24]. The phase transition occurs at 140 K resulting to orthorhombic space group Fmmm. The considered cluster model is $[Ba_4FeAs_4]^{2-}$ (see Figure 7.2(c)).

SmOFeAs has a tetragonal structure (P4/nmm) with alternating layers of Fe-As and Sm-O in which these layers are well separated [23]. These compounds experience a structural phase transition at around 150 K, resulting in the orthorhombic symmetry of the Cmma space group. The considered cluster model is $[Sm_4FeAs_4O_4]^{6-}$ (see Figure 7.2(d)).

The MIS calculations were carried out using the B2-PLYP functional and HFC (hyperfine coupling constant) calculations using the B3LYP functional. The 24s12p9d basis set of Partridge with a set of polarization functions taken from TZVpp basis set of Ahlrichs and May is used for iron, which is in the uncontracted form. For As/Se the augmented correlation consistent double-zeta (aug-cc-pVDZ) basis set of Dunning is used. The Li^{I} and Ba^{II} were modeled by the respective Stuttgart effective core potentials (ECPs). Sm^{III} is modeled by the Al^{III} ECPs, having same valence state and nearly identical ionic radii the use of Al^{III} helps to avoid the complexity of including f electrons in Sm. All the calculations were done in embedded cluster approach, which is explained in Chapter 4.

The Mössbauer isomer shift calculations were carried out using the linear response formalism, as described in the earlier chapters. The contact density near the nucleus is calculated according to Eqn. 2.44, and the MIS are calculated using the calibration constant $\alpha(^{57}\text{Fe}) = -0.306 \pm 0.009\ a_0^3$ mm s^{-1} obtained with the use of the B2-PLYP functional in Chapter 5 (using Eqn. 3.1).

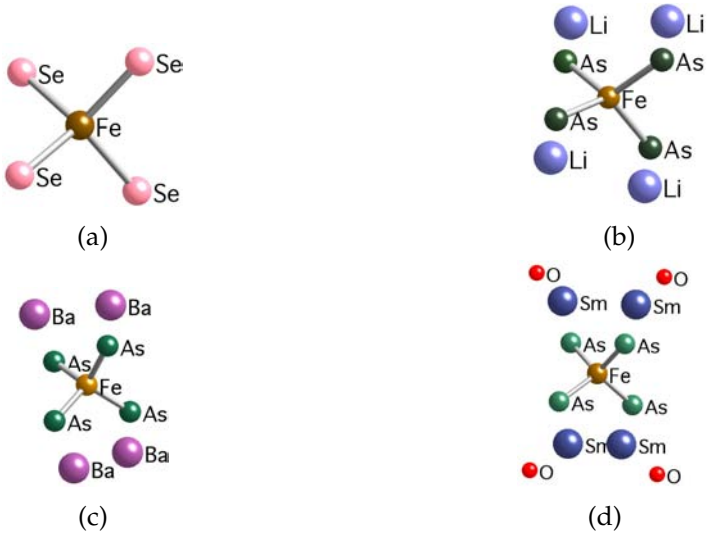

Figure 7.2: *The clusters studied, (a)$FeSe_4$ (b) Li_4FeAs_4 (c) Ba_4FeAs_4 (d) $Sm_4FeAs_4O_4$.*

The details of the HFC calculations are given below. The part of the ESR spin Hamiltonian referring to hyperfine coupling is usually written as [136],

$$H_K^{hf} = S.A_K.I_K \tag{7.1}$$

The isotropic Fermi-contact term A^{FC}, and the anisotropic dipolar coupling A^{dip}, can be calculated using the Breit-Pauli Hamiltonian and a vector potential corresponding to a point-like magnetic dipole moment of nucleus K. Within a single-determinantal LCAO approach, these may be expressed as [136],

$$A_K^{iso} = A_K^{FC} = \frac{4\pi}{3}\alpha^2 g_e \gamma_K \frac{1}{2 < S_Z > \mu,\nu} \sum P_{\mu,\nu}^{\alpha-\beta} < \chi_\mu|\delta(r_K)|\chi_\nu > \tag{7.2}$$

$$A_{K,\mu,\nu}^{dip} = \frac{1}{2}\alpha^2 g_e g_K \gamma_K \frac{1}{2 < S_Z > \mu,\nu} \sum P_{\mu,\nu}^{\alpha-\beta} < \chi_\mu|r_K^{-5}(r_K^2\delta_{\mu,\nu} - 3r_{K,\nu}r_{K,\nu})|\chi_\nu > \tag{7.3}$$

where γ_K is the gyromagnetic ratio of nucleus K, and g_e is the free-electron g value (2.002319...). $<S_Z>$ is the maximum value of the spin projection and $P_{\mu,\nu}{}^{\alpha-\beta}$ is the spin density matrix in the atomic orbital basis $\{\chi_\mu\}$. A^{FC} and A^{dip} contribute to the nonrelativistic part of the HFC tensor. The details on the theory behind HFC calculations can be obtained from Ref. [136] and the references therein.The dominant SO corrections to the calculations are included as a second order correction [136].

The total A tensor is expressed as,

$$A_K = A_K^{NR} + A_K^{SO} \tag{7.4}$$

where A_K^{SO} is the spin-orbit correction to A, which may be obtained in terms of an isotropic pseudocontact (PC) and traceless dipolar ("dip,2") term.

$$A_K^{SO} = A_K^{PC} + A_K^{dip,2} \tag{7.5}$$

The HFC calculations were done with the use of the MAG-ReSpect program package in which the coupled perturbed Kohn-Sham algorithm with the inclusion of spin-orbit interaction is implemented [137]. The calculations are done with iron spin S = 1 state.

Generally in physics and mathematics, uniaxiality and asymmetry are two characteristics of a symmetric second-rank tensor in three-dimensional Euclidean space, describing its directional asymmetry. Let A denote a second-rank tensor in R^3, which can be represented by a 3-by-3 matrix. Assuming that A is symmetric, A has three real eigenvalues, which are denoted by A_{xx}, A_{yy} and A_{zz}. Assume that they are ordered such that :$A_{xx} < A_{yy} < A_{zz}$, then uniaxiality ΔA is represented as $2A_{zz}$ - (A_{xx} + A_{yy}) and asymmetry as δA = (A_{yy} - A_{zz}). In analogy with this, the hyperfine matrix can also be used to derive uniaxiality

and asymmetry parameters. Taking the largest diagonal element of the A-tensor as A_1 and the smallest as A_3, the dipolar (anisotropic) components can be used to derive the uniaxiality b_0 = [A_1 - (A_2 + A_3)/2]/3 and the asymmetry c_0 = (|A_2| - |A_3|)/2 parameters.

7.3 Results and Discussion

In this chapter, the results of the MIS and HFC calculations carried out for the aforementioned iron compounds are presented and analysed. The emphasis is to study the influence of the structural phase transitions and the degree of doping with other elements on the hyperfine structure parameters, MIS and HFC.

7.3.1 MIS calculations

The contact densities calculated using Eqn. 2.44 for the iron based clusters presented above are given in Table 7.1. The isomer shifts can be computed according to Eqn. 3.1 using the given contact densities along with the calibration constant $\alpha(^{57}\text{Fe}) = -0.306 \pm 0.009\ a_0^3$ mm s^{-1} from the parametrizations in Chapter 5. Figure 7.3 plots the calculated relative shift, $\Delta\delta^x = \delta^x - \delta^{ref}$ (in mm/s) (ref is [$K_4Fe(CN)_6$]) for both HT and LT phases.

The isomer shifts in Table 7.1 show reasonable agreement with the experimental shifts. It is gratifying that the calculations done using small cluster models of the representative crystal structures could effectively reproduce the experimental results.

It is seen from the results in Table 7.1 that the overall differences in the calculated contact densities and corresponding $\Delta\delta$s within each temperature phase is in smaller range ($\Delta\delta_{HT} \approx 0.02$ mm/s, $\Delta\delta_{LT} \approx$

Table 7.1: *^{57}Fe electron contact densities according to Eqn. 2.44 of the iron based superconductors.*

	HT			LT		
	ρ^a	$\delta_{calc}{}^b$	$\delta_{exp.}{}^b$	ρ^a	$\delta_{calc.}{}^b$	$\delta_{exp.}{}^b$
$FeSe_4$	54.20	0.51	0.53[c]	54.09	0.54	0.54[c]
Li_4FeAs_4	54.22	0.49	0.44[d]			
Ba_4FeAs_4	54.19	0.51	0.29[e]	54.02	0.56	0.42[e]
$Sm_4FeAs_4O_4$	54.17	0.52	0.43[f]	54.02	0.56	0.57[f]

[a] A large constant of 15000 $a_0{}^{-3}$ has been subtracted from all the values.
[b] with respect to $[K_4Fe(CN)_6]$)
[c] from Ref. [138]
[d] from Ref. [139]
[e] from Ref. [24]
[f] for LaFeAsO, from Ref. [140]

0.02 mm/s). All the compounds with the same crystal structure have nearly identical contact densities and isomer shifts irrespective of the difference in the outer coordination sphere of ^{57}Fe in different types of superconductors, such as type 1111, 122, 111 and 011. The basic structure of these compounds is $FeAs_4$ tetrahedra separated by Li/Ba/SmO layers in 111, 122 and 1111 types of compounds. In the present calculations these inter layers are represented by ECPs as explained in the earlier section, for computational simplicity. This could be responsible for the nearly identical δs for the same crystalline phase (HT or LT) of these compounds. Therefore, one can expect to see a more precise distinction between different types of compounds by computing Li/Ba/Sm with all electron basis sets.

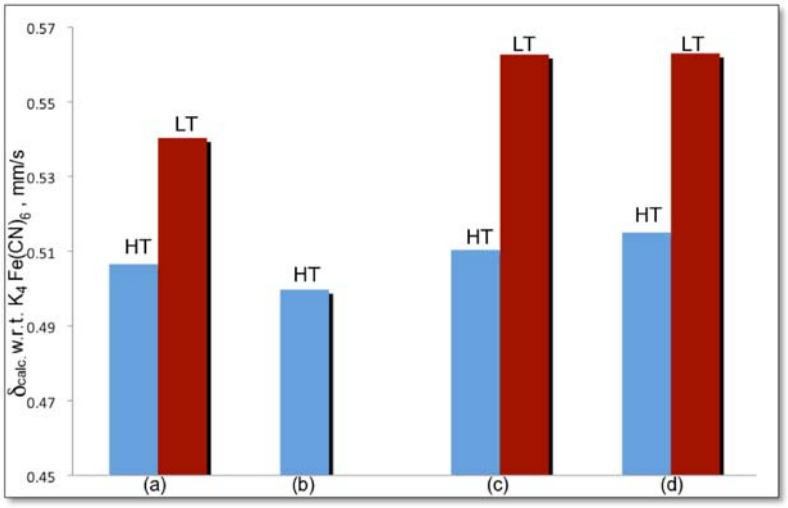

Figure 7.3: *The $\Delta\delta$ for HT (298 K) and LT (5 K) for a) $FeSe_4$, b) Li_4FeAs_4, c) Ba_4FeAs_4 and d) $Sm_4FeAs_4O_4$.*

The general trend of the isomer shift variation between the HT and LT phase indicate that the electronic structure variations in these compounds are similar (see Table 7.1 and Figure 7.3). Figure 7.3 shows a clear jump of isomer shift with tetragonal - orthorhombic transition in all the compounds, for FeSe_4 the $\Delta\delta$ is +0.05 mm/s corresponding to a decrease of ^{57}Fe electron contact density of *ca.* 0.17 a_0^{-3} with the lowering of temperature. This feature, which is characteristic for all the compounds studied can be suggested as a diagnostic test for the local chemical environment of the ^{57}Fe ions.

The superconductivity emerges in 1111 & 122 types of compounds with the electron or hole doping of the parent compounds. Therefore, it is interesting to study the MIS variation with the doping/chemical substitution of these compounds. Figure 7.5 shows the MIS variation for the HT structures with various levels of chemical substitution for 3 types of compounds, $FeSe_4$, Ba_4FeAs_4 and $Sm_4FeAs_4O_4$. The stud-

Figure 7.4: *The substitution of Se with S on $FeSe_4$ clusters, (a)$FeSe_4$ (b) $FeSe_3S$ (c) $FeSe_2S_2$ (d) $FeSeS_3$.*

ied clusters are, a) $FeSe_4$, Se substituted partially with S, ie, $FeSe_3S$, $FeSe_2S_2$, $FeSeS_3$ b) Ba_4FeAs_4, Ba substituted with K, Ba_3KFeAs_4, Ba_2K_2-$FeAs_4$, BaK_3FeAs_4 and c) $Sm_4FeAs_4O_4$, O substituted with F, $Sm_4FeAs_4O_3F$, $Sm_4FeAs_4O_2F_2$, $Sm_4FeAs_4OF_3$. To get a general idea of the chemical

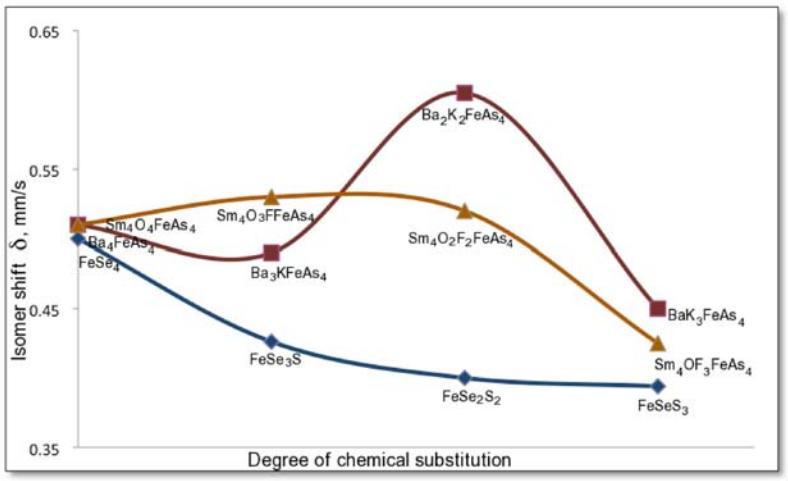

Figure 7.5: *The dependence of MIS on doping/chemical substitution*

substitutions carried out in this chapter, a pictorial representation of Se substituted with S is given in Figure 7.4. The results given in Figure 7.5 show that substitution of S for Se in $FeSe_4$ makes a decrease in the isomer shift, which is in the range of 0.11 mm/s. However, no such trends are seen for Ba_4FeAs_4 and $Sm_4FeAs_4O_4$. The reason could be that the chemical substitution in the first coordination sphere of ^{57}Fe

has stronger influence on the isomer shift than that of the substitution on interlayer atoms, Ba or O. However, if one neglects the bump in $BaFeAs_4$ plot ($Ba_2K_2FeAs_4$), the overall variation is in the decrease of MIS with K doping which is consistent with the earlier reported results [24].

Figure 7.5 shows that the range of variation of MIS is relatively low, *ca.* 0.11 mm/s for $FeSe_4$. In experiments, superconductivity emerges with less than 3% of doping/chemical substitution in these compounds. Hence this $\Delta\delta$ could be smaller than 0.11 mm/s under experimental conditions, which would indicate that the contact density variation near ^{57}Fe in these types of compounds is relatively low with the electron/hole doping.

7.3.2 HFC calculations

Before starting with the calculations on iron based superconductors, the B3LYP functional and the basis sets specified earlier are tested in the calculation of the hyperfine structure constants of complexes for which the experimental data are available. The results along with the references for the geometries are given in Table 7.2. In most of the cases the calculated isotropic HFC values (A_{iso}) are underestimated. The SO contributions are given for $Fe^{II}SR_3$ and $Fe^{III}Az$. For the latter compound, the inclusion of SO improves the agreement with experiment.

The underestimation of A_{iso} values on compounds such as Fe^{III}MAC, Fe^{IV}MAC *etc* are seen by Sinnecker, Slep, Bill and Neese in Ref. [141]. They applied a scaling factor f = 1.81 to the computed Fermi Contact terms on the iron complexes with small values of A_{iso}. In Figure 7.6, the calculated isotropic HFC is plotted against the experi-

Table 7.2: *The hyperfine coupling constants (MHz) for the reference compounds.*

		A_{aniso}(calc.)			A_{aniso}(exp.)	
	A_{iso}(calc.)	b_0	c_0	A_{iso} (exp.)	b_0	c_0
$Fe^{II}SR_3$[a]	-9.93	-3.83	0.10	-11.8	-7.3	0.00
	(-8.49)[b]	(-5.47)	(0.13)			
Fe^{II}PorOAc[a]	-13.56	2.73	0.59	-21.8	1.7	0.00
Fe^{III}Az[a]	-15.49	-1.84	1.26	-13.5	-10.80	0.90
	(-12.50)	(-4.55)	(1.30)			
Fe^{III}MAC[a]	-6.77	5.01	2.55	-15.40	11.15	3.75
$Fe^{III}PO_4$[c]	-23.91	-4.21	3.68	-28.2	...	...
$Fe^{III}(H_2O)_6$[a]	-19.89	-0.22	0.12	-32.60	...	...
Fe^{IV}MAC[a]	-11.11	2.35	0.10	-20.00	2.65	2.05

[a] See Ref. [141] and the references therein.
[b] In paranthesis, the results with SO coupling
[c] Ref. [142]

mental isotropic HFC, where for $Fe^{II}SR_3$ and Fe^{III}Az, the A_{iso} values represents the B3LYP values including SO couplings. For all other complexes the B3LYP values were scaled by a factor of 1.81 (Ref. [141]). Thus, the agreement with experimental isotropic HFC values are improved.

In Table 7.2 the calculated anisotropic hyperfine coupling constants along with experimental values are given in terms of uniaxiality b_0

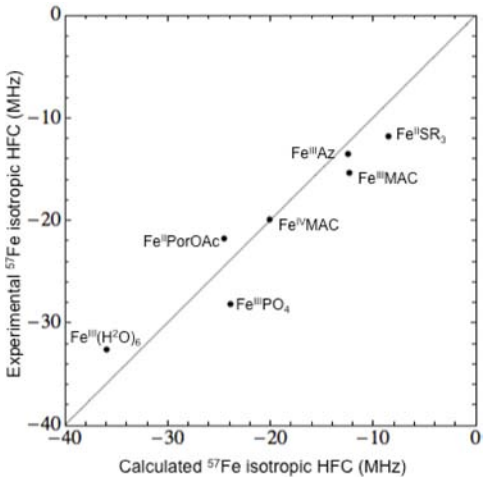

Figure 7.6: *Calculated ^{57}Fe Isotropic hyperfine coupling constants vs. experimental hyperfine coupling constants for the reference compounds (see text for details).*

and asymmetry c_0 parameters. For $Fe^{II}SR_3$ and $Fe^{III}Az$, the inclusion of SO corrections improves the agreement of b_0 and c_0 values with experiment. The overall agreement of the calculated b_0 and c_0 values with experimental values gave us confidence to use B3LYP functional and the proposed basis sets for the calculations of the iron based superconductors.

The hybrid functional with increased percentage of HF exchange, such as BH&HLYP are tested on selected compounds in order to analyse their performance. The results showed an increase of the isotropic HFC values of *ca.*4-5 MHz in magnitude and hence it can improve the agreement with experimental values. However, the SO contribution within the BH&HLYP functional for one of the reference compound produces a higher positive value, making the overall isotropic HFC value similar in magnitude to the B3LYP result. Therefore, the calculations here are done within B3LYP functional only.

The HFCs with and without SO corrections are given in Table 7.3 for the considered iron based superconductors. For all the compounds, there is a slight decrease of the A_{iso} values with the tetragonal-orthorhombic phase transition. The trend is similar for the A_{iso} values including SO corrections.

The isotropic HFC values (A_{iso}) without including SO corrections differ by *ca.*1 MHz for the HT and LT phases (see Table 7.3). However, the SO corrections bring in a clear distinction between the different types of compounds. Based on the results, the iron-based superconductors can be divided into 3 groups, a) $FeSe_4$ and Li_4FeAs_4 b) Ba_4FeAs_4 and c) $Sm_4O_4FeAs_4$. The first group which has relatively short interlayer separation (see Figure 7.1(a,b)), has lower A_{iso} values, whereas for b and c groups the A_{iso} values increase. With the increase in the inter layer separation, from 011 to 1111 types, the spin density near the ^{57}Fe increases, which is evident from the calculations including SO corrections. The SO contributions account for up to 30 % of the hyperfine coupling constant, therefore it is crucial for the understanding of the magnetic hyperfine coupling constants of these compounds.

The anisotropic contributions of the hyperfine coupling constants represented by the uniaxiality b_0 and asymmetry c_0 are given in Table 7.3. The results show that there is an increase of the uniaxiality in all the compounds with the tetragonal-orthorhombic phase transition. The asymmetry c_0 increases from 011 to 1111 types (see Table7.3), indicating a decrease of the tetrahedral symmetry of FeX_4 (X = Se/As) in these compounds from 011 to 1111 types.

An apparent small magnetic moment per iron atom ($\mu \approx 0.4\mu$B) was reported for pnictides of the 1111 type, which is much less than in 122 compounds ($\approx 0.9\ \mu$B) and they are much smaller than the DFT

Table 7.3: *Hyperfine coupling constants (MHz) for the iron compounds studied both including and excluding the SO effects at B3LYP level of theory.*

	A_{aniso}			A_{aniso}(SO)		
	A_{iso}	b_0	c_0	A_{iso} (SO)	b_0	c_0
$FeSe_4$-HT	-10.93	-4.14	0.01	-7.77	-5.86	0.01
$FeSe_4$-LT	-10.55	-4.18	0.17	-7.50	-6.04	0.01
Li_4FeAs_4-HT	-11.90	-3.32	0.44	-8.61	-4.71	0.525
Ba_4FeAs_4-HT	-11.51	5.08	0.95	-9.31	5.78	2.625
Ba_4FeAs_4-LT	-10.96	5.13	1.27	-9.03	6.09	2.785
$Sm_4O_4FeAs_4$-HT	-11.86	3.17	2.09	-10.40	4.33	2.33
$Sm_4O_4FeAs_4$-LT	-11.33	3.25	2.98	-10.02	4.84	2.61

predicted value ($\approx$ 2 μB) [144, 145]. The difference in the magnetic moment between 1111 type and 122 type could be that the interlayer coupling of FeAs layers is stronger in 122 compounds than 1111 compounds because the interlayer distance in 122 compounds is significantly shorter than 1111-compounds (see Figure 7.1). There are several factors contributing to the reduction of the observed magnetic moment, among which can be mentioned : i) the effect of itinerant electrons, the DFT calculations are done on a small magnetic unit cell and the interactions with the itinerant electrons are not considered, therefore the moment obtained by DFT is the bare moment of each Fe ion, and ii) the effect of SO coupling, the SO coupling induces singlet-triplet mixing which can reduce the observed magnetic moment per

iron atom. In the present calculations, it is seen that the influence of SO corrections on A_{iso} values are relatively strong (up to *ca* 30 %) and there is a reduction of the absolute values indicating a reduction in the spin density (see Table 7.3). Therefore, it can be inferred that with the inclusion of SO corrections, there is singlet-triplet mixing and corresponding decrease in spin density.

The effect of chemical substitution or electron doping on the calculated isotropic hyperfine coupling constants are evaluated for a number of representative clusters of a) $FeSe_4$ and b) Li_4FeAs_4 and c) Sm_4O_4-$FeAs_4$. For $FeSe_4$, partial substitution of Se with isovalent S atoms, ie, $FeSe_3S$, $FeSe_2S_2$; Li_4FeAs_4 where a partial substitution of Li with K, Li_3KFeAs_4 and $Li_2K_2FeAs_4$; $Sm_4O_4FeAs_4$ where a partial substitution of O with F, $Sm_4O_3FFeAs_4$ and $Sm_4O_2F_2FeAs_4$ are carried out. The results are plotted in Figure 7.7. Similar to the MIS calculations, substitution of the interlayer atoms, ie, O with F in $Sm_4O_4FeAs_4$ and Li with K in Li_4FeAs_4, does not show a clear trend in the A_{iso} variations, whereas the substitution in the direct co-ordination sphere of ^{57}Fe, ie, Se with S makes a slight increment in the magnitude of A_{iso} values. All these three classes (a-c) show isotropic HFC values (A_{iso}) within 0.25 MHz variation with the chemical substitutions, suggesting an independence of A_{iso} values on the degree of chemical substitution.

However, the inclusion of SO corrections for Li_3KFeAs_4 gives an A_{iso} value of -9.38 MHz, whereas the A_{iso} for Li_4FeAs_4 is -8.61 MHz, which makes a noticeable increase in the magnitude of the hyperfine coupling constant indicating an increase of spin density near ^{57}Fe nucleus with the K- doping. Therefore, it is clear that the distortion in the local geometry and changes in the spin density near ^{57}Fe with the electron/hole doping in these compounds can only be accurately studied by the calculations including the SO corrections.

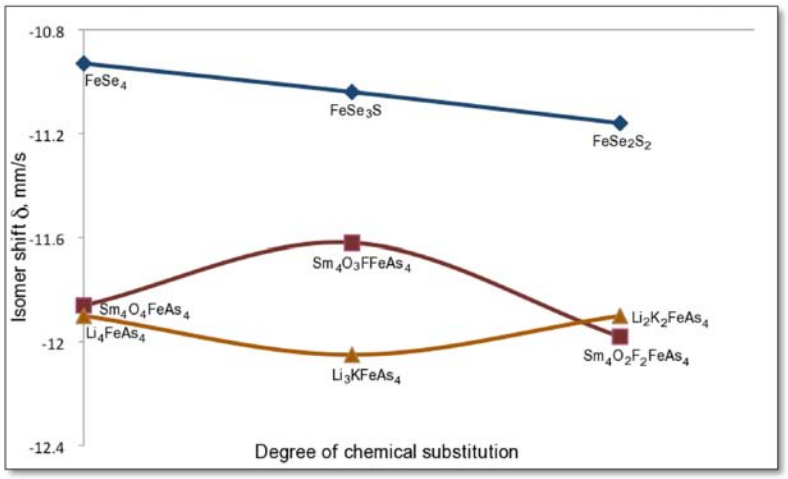

Figure 7.7: *The dependence of A_{iso} on doping/chemical substitution*

7.4 Conclusion

The knowledge of the local electronic structure in iron-based superconductors should help to understand the interplay between the structure and the emergence of superconductivity in these compounds. In the present chapter, the iron based high temperature superconductors, FeSe, LiFeAs, $BaFe_2As_2$ and SmOFeAs are investigated in order to understand the variation of the isomer shifts and the hyperfine coupling constants with tetragonal-orthorhombic phase transition.

The isomer shift calculations within the linear response approach have been done using double hybrid density functional method (B2-PLYP). The relative ^{57}Fe isomer shifts calculated with respect to [K_4Fe-(CN)$_6$] for tetragonal/orthorhombic crystal structure are within a variation of less than 10% irrespective of the different chemical environments. The calculations have shown that the electron contact density near the ^{57}Fe nucleus reduces and correspondingly the isomer shift increases with the tetragonal - orthorhombic phase transition. This

variation can be taken as a criterion for monitoring the local chemical environment around the resonating nuclei, in different temperature phases and during phase transitions.

The hyperfine coupling constant calculations done with the B3LYP functional show that the tetragonal-orthorhombic transition produces only a slight variation in the local spin moment near the nucleus, and consequently in the isotropic hyperfine coupling constants, A_{iso}. However, including the SO corrections in the calculations reduces the spin density near the ^{57}Fe nucleus, and the A_{iso} values. The SO corrections scale up to 30 % of the calculated A_{iso} values, making a distinction between different types of the superconductors. It has been observed that with the increase in the interlayer separation, ie, from 011 to 1111 types, there is an increase of A_{iso} values. The uniaxiality of the A-tensor of these compounds increases with the tetragonal-orthorhombic phase transitions.

The dependence of MIS and HFC on doping has shown that the influence is stronger with the chemical substitution in the immediate coordination sphere of ^{57}Fe and it is less noticeable with the doping/chemical substitution in the inter layers such as Li/Ba/SmO in 111, 122, 1111 types of compounds.

The present chapter investigates on the local chemical environment near the ^{57}Fe nucleus in the iron based superconductors within the scope of the Mössbauer spectroscopy parameters, the isomer shift and hyperfine coupling constant. The results indicate that these (MIS and HFC) are good tools to get an insight into the variation of the electronic structure and magnetic spin densities under phase transition and upon doping/chemical substitutions in the coordination sphere of ^{57}Fe. Therefore, these tools can effectively be used for monitoring the structure of these compounds and in a wider perspective con-

tribute to a better understanding of the mechanism behind superconductivity in these compounds.